CCFE
CULHAM CENTRE FOR FUSION ENERGY

UK Atomic Energy Authority

UKAEA-CCFE-PR(21)67

D.M.A.Taylor, M.J.Mantsinen, D.Gallart, J.Manyer,
JET contributors

Effect of inclusion of pitch-angle dependence on a simplified model of RF deposition in tokamak plasma

Effect of inclusion of pitch-angle dependence on a simplified model of RF deposition in tokamak plasma

D.M.A.Taylor, M.J.Mantsinen, D.Gallart, J.Manyer, JET contributors

This is a preprint of a paper submitted for publication in Nuclear Fusion

IOP PublishingJournal Title
Journal **XX** (XXXX) XXXXXX https://doi.org/XXXX/XXXX

Effect of inclusion of pitch-angle dependence on a simplified model of RF deposition in tokamak plasma

D. M. A. Taylor[1], M. J. Mantsinen[2,3], D. Gallart[2], J. Manyer[2], and JET contributors†

[1] United Kingdom Atomic Energy Authority, Culham Centre for Fusion Energy, Culham Science Centre, Abingdon, Oxon, United Kingdom OX14 3DB, UK
[2] Barcelona Supercomputing Centre (BSC), Barcelona, Spain
[3] ICREA, Barcelona, Spain
† See the author list of "Overview of JET results for optimising ITER operation" by J. Mailloux et al. to be published in Nuclear Fusion Special issue: Overview and Summary Papers from the 28th Fusion Energy Conference (Nice, France, 10-15 May 2021)

E-mail: david.taylor@ukaea.uk

Received xxxxxx
Accepted for publication xxxxxx
Published xxxxxx

Abstract

Using the PION ICRH modelling code on JET tokamak pulses, the effect of including pitch angle dependence within the RF diffusion operator is investigated. This is found to be of greatest importance to the fast ion particle distribution function in cases of higher harmonic heating and lower heating ion mass, resulting in faster drop-off of the distribution's high energy tail and non-linear alterations to ion species power partition. ITER scenario operational parameters are also considered, and this improved treatment is shown to benefit predictions of ITER scenarios with second harmonic hydrogen heating, according to our predictions. PION's combination of benchmarked simplified wave physics and Fokker-Planck treatment offers modelling advantages.

Keywords: tokamak, ICRF, ICRH, PION, fast ions, neutron spectroscopy, JET, ITER

1. Introduction

Radio frequency auxiliary heating of tokamak plasma in the ion cyclotron frequency range is now a common technique for a variety of plasma ion compositions, used on many present and planned toroidal plasma devices [1-3].

PION is a well-established computing tool that evolves the time-evolution of ICRH power absorption and the distribution functions of the resonant ions in a self-consistent way [4, 5]. Extensively validated against experimental data on JET [5-13], AUG [14-17], DIII-D [18], and WEST (formerly Tore Supra) [19, 20] for many minority and majority heating schemes, its models use simplified physics, making it a versatile and relatively fast solver suitable for prompt analysis. This speed sees it implemented as part of the automated data processing chain at JET (including an intershot version). It has been installed in the ITER Integrated Modelling and Analysis Suite (IMAS), enabling integrated predictive modelling of ITER plasmas [21].

ICRH modelling is relatively complex, due to the need to solve Fokker-Planck and wave equations in a self-consistent way. PION's principal physics simplifications are twofold: firstly, the wave power deposition is taken to be a superposition of strong and weak absorption limit cases; secondly, the Fokker-Planck equation is modelled as a function of flux surface, scalar velocity, and time only.

We consider here comparisons of PION fast ion distribution functions with diagnostic results from the 2.5 MeV TOFOR neutron spectrometer and the High Energy Neutral Particle Analyser, revisiting PION modelling for pulses previously published by Salmi [11] and Schneider [22].

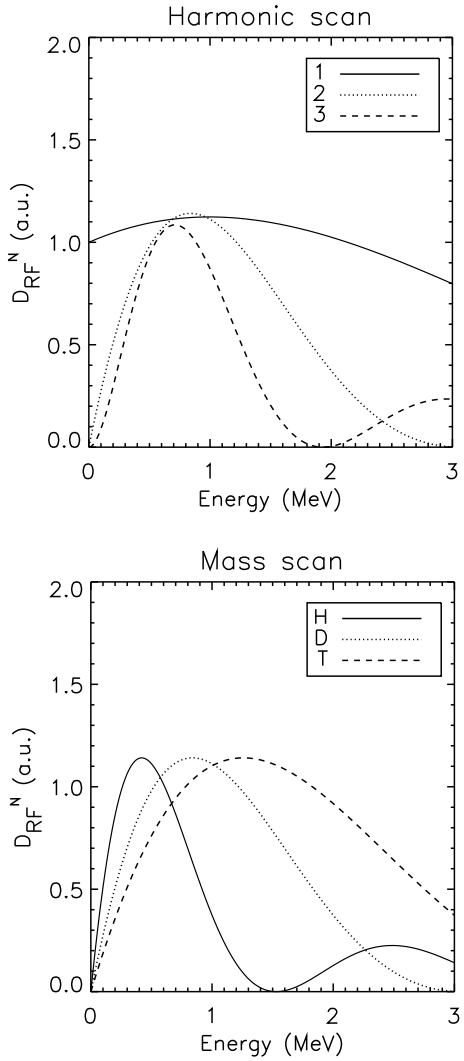

Figure 1: Variation of RF diffusion coefficient D_{RF}^N with energy for (a) harmonic number n with deuterium heating, and (b) ion mass with 2nd harmonic heating. Parameters: $k_\perp = 56.6\ m^{-1}$, $\frac{E_+}{E_-} = 0.43$, $\omega_c = 51.5\ MHz$.

This paper presents the effect of including pitch angle dependence within the RF diffusion operator calculation. This contrasts with earlier calculations, made using pitch angle averaging. These improvements have only small effect in most modelling cases. For example, in the common situation of modelling a fundamental resonance, little change is expected. However, there are modelling cases where we can better match observations for some JET experimental regimes. We note the cases of second harmonic hydrogen heating and third harmonic deuterium heating, where the higher harmonic brings the minimum in the RF diffusion coefficient down to an energy value whose particle distribution is experimentally measurable. Physically, this minimum expresses the energy value at which resonant Larmor radius accelerations and decelerations cancel [6], as derived in Kennel-Engelmann theory [23]. We also note significant changes to the power absorption of heated ion species due to the changed diffusion coefficient.

To illustrate these tendencies, Fig. 1 shows the RF diffusion coefficient $D_{RF}^N(v)$ for a single resonance point, with v assumed to be entirely perpendicular, resonant frequency held constant, and scaled to display values around unity. Under these conditions, the expression for the diffusion coefficient takes the simplified form shown in Eq. 1, as given in [6].

$$D_{RF}^N \propto \left| E_+ J_{n-1}\left(\frac{k_\perp v}{\omega_c}\right) + E_- J_{n+1}\left(\frac{k_\perp v}{\omega_c}\right)\right|^2 \qquad (1)$$

Here J_n is a Bessel function of the first kind of order *n*, *N* is the toroidal mode number, *n* is the ion cyclotron harmonic, ω is the frequency of the launched wave, E_+ and E_- are respectively the left and right hand electric field components, ω_c is the ion cyclotron frequency, *k* is the wavenumber, *v* the velocity, and the subscript $\perp$ denotes the component of a quantity that is perpendicular to the magnetic field. Physically, the RF diffusion coefficient is proportional to the kick in energy given to the perpendicular velocity [24], and its tail corresponds to high energy absorption.

Fig. 1a shows the functional dependence on harmonic number, which enters only in the Bessel function order. In consequence, there is marked similarity between the dependence of Bessel functions on order and this dependence on harmonic number. We observe the behaviour in the limit of zero velocity, where the presence of a J_0 component in the fundamental heating expression implies substantial heating at low energies that is not present for higher harmonic heating, as shown in Fig. 1a. We also observe the decreasing energy value of the function minimum as harmonic number increases to a value of 3, a characteristic not easily analytically provable, but one readily numerically demonstrated for a range of E_+/E_- exceeding experimental reality. This decrease of minimum position points to the increased importance of the method given here in second and third harmonic heating schemes.

Fig. 1b shows the functional dependence on ion mass, which enters in the dependency on cyclotron frequency and the scaling from velocity to kinetic energy. The effect is of a linear stretching in energy; the energy position of the minimum is at twice the value for deuterium as for hydrogen, and three times for tritium.

The planned list of operational scenarios for ITER contains several that use second harmonic heating, and will also include plasmas with different ion isotope masses. So we see a natural relevance of this work to the experiments that will employ these scenarios, for which we expect the distribution function tail shape to be of importance.

In this paper, we will present firstly the necessary theoretical background, continue by comparing results, and conclude with some general remarks.

2. Theoretical background

2.1 PION overview

PION [4, 5] is a time-dependent code that models the deposition of ICRH power into tokamak plasma. Its attractiveness as a modelling tool lies in its tested simplifications of the full wave problem, allowing it to return results relatively rapidly for the full duration of a plasma discharge.

At each time step, it iterates two tasks. First, it calculates the power deposition. This is done by Fourier decomposition into individual toroidal modes. The power coupled to each mode is calculated according to the model described in [6], which was partly obtained by comparison with results from the full wave code LION [25, 26]. This model takes the deposited power as the superposition of weak and strong absorptions, partitioned as a function of the single pass absorption coefficient across the midplane [4]. The power lost to mode conversion is removed from the coupled power by using the Budden formula [27] to treat it as resonance absorption in a planar geometry.

Having modelled the deposition, PION then uses a one-dimensional Fokker-Planck equation to time-evolve the ion distribution function $f(v)$, calculating the power partition between heated species. The dielectric tensor components are updated with the output of this second part of the algorithm loop, and then fed back into the start of the loop process.

2.2 General theory background

For completeness we give the full three-dimensional description, then restrict to the used model.

. We start from the general form of an orbit-averaged Fokker-Planck equation [28], Eq. 2:

$$\frac{\partial f}{\partial t} = \langle C(f)\rangle + \langle Q(f)\rangle \qquad (2)$$

where $<>$ denotes an average over the drift orbit, *t* is time, f is a particle distribution function, C is a collision operator, and Q is a quasi-linear diffusion operator describing ICRH wave-particle interaction. When we average over orbits, the second term becomes

$$\langle Q(f)\rangle = \sum_N L_N(D_{RF}^N L_N f) \qquad (3)$$

where L_N is a co-ordinate transformation operator expressed in terms of a set of invariants. Here again *N* is the toroidal wavenumber, and D_{RF}^N is the diffusion coefficient for that *N*. Under orbit averaging, this description is three-dimensional, requiring three invariants to relate Q to D_{RF}. Following [29] and [5], we use the set (E, Λ, P_φ), where E is the ion energy, $\Lambda = v_\perp^2 B_0/v^2 B$, and P_φ is the toroidal ion angular momentum $mRv_\phi + Ze\psi_p$. Here *v* is the ion velocity, the subscripts ϕ and $\perp$ denote respectively the components of a quantity that are toroidal and perpendicular to the magnetic field B, B_0 is the axial magnetic field, m is the ion mass, *R* is the major radius, Ze is the ion charge, and ψ_p is the poloidal magnetic flux. This permits the representation

$$L_N = \frac{\partial}{\partial E} + \frac{n\omega_{c0} - \Lambda\omega}{\omega E}\frac{\partial}{\partial \Lambda} + \frac{N}{\omega}\frac{\partial}{\partial P_\varphi} \qquad (4)$$

with the diffusion coefficient D_{RF}^N taking the form [4]

$$D_{RF}^N = \frac{1}{4\omega^2}\sum_R \frac{(Ze)^2}{|n\dot{\omega}_{cR}|} v_{\perp R}^2 \left| E_+ J_{n-1}\left(\frac{k_\perp v_{\perp R}}{\omega_{cR}}\right) + E_- J_{n+1}\left(\frac{k_\perp v_{\perp R}}{\omega_{cR}}\right)\right|^2 \qquad (5)$$

where the subscript *R* denotes resonance points. As before, *n* is the ion cyclotron harmonic, ω is the frequency of the launched wave, E_+ and E_- are respectively the left and right hand electric field components, ω_{c0} is the ion cyclotron frequency at the magnetic axis, ω_{cR} is the ion cyclotron frequency at the resonance point, and *k* is the wavenumber.

2.3 Development

Under PION's formalism, which follows [30], the Fokker-Planck equation becomes

$$\frac{\partial f}{\partial t} = \frac{1}{v^2}\frac{\partial}{\partial v}\left[-\alpha v^2 f(v) + \frac{1}{2}\frac{\partial}{\partial v}(\beta v^2 f(v))\right] + \frac{1}{v^2}\frac{\partial}{\partial v}\left[v^2 D_{RF}\frac{\partial f(v)}{\partial v}\right] \qquad (6)$$

where α and β are parameters arising from the model that describes the collisional term [31].

The second right hand side term of Eq. 6 details how the coefficient D_{RF} enters the model. Following [30], PION has modelled D_{RF} in pitch angle averaged fashion. This is a good assumption for the commonly-modelled case of fundamental heating, but less good for higher harmonic heating, due to the presence in expressions for D_{RF} of Bessel functions and their dependence on the harmonic number and ion mass.

In this paper we present the results of modelling D_{RF} with a resolved pitch angle. Following [32], we use the ansatz

$$f(v,\mu) = F(v)\frac{e^{-\left(\frac{\mu}{\Delta\mu(v)}\right)^2}}{\sqrt{\pi}\Delta\mu(v)\,\mathrm{erf}\left(\frac{1}{\Delta\mu(v)}\right)} \qquad (7)$$

where erf is the Gaussian error function, $F(v)$ is the pitch angle averaged distribution function, $f(v,\mu)$ is the pitch angle resolved distribution function, $\mu = v_\parallel/v$ is the cosine of the pitch angle of the ion relative to the background magnetic field, and the width of the exponential $\Delta\mu(v)$ characterises the dependence of the distribution on the pitch angle. The valid range of the distribution is bounded in μ by ± 1, with the integral of the distributed function over this range being $\int_{-1}^{1} f(v,\mu)d\mu = F(v)$. When $\mu = 0$, the ion pitch angle is perpendicular to the field line, and the angle-averaged case is recovered. In this work, the use of the variable μ in PION is algorithmically restricted to the calculation of *f* and D_{RF}. The returned distribution function is calculated internally as a function of both *v* and μ, but then used as a function of *v* only.

The distribution width $\Delta\mu(v)$ is calculated from the velocity distribution by equating expressions for the effective pitch angle $\mu_{eff}^2(v)$, a quantity that we define as the distribution-averaged μ^2. We see by integration of its definition that this is equal to

$$\frac{\int_{-1}^{1}\mu^2 f(v,\mu)d\mu}{\int_{-1}^{1} f(v,\mu)d\mu} = \frac{[\Delta\mu(v)]^2}{2} - \frac{\Delta\mu(v)}{\sqrt{\pi}}\frac{e^{-\left(\frac{1}{\Delta\mu(v)}\right)^2}}{\mathrm{erf}\left(\frac{1}{\Delta\mu(v)}\right)} \qquad (8)$$

According to Ref. [33] $\mu_{eff}^2(v)$ is also approximately equal to

$$\frac{1}{3}\frac{1+v_n^2}{1+v_n^2+v_n^4} \qquad (9)$$

where $v_n = 2v/v_\gamma$, v_γ being the characteristic velocity associated with pitch angle scattering [29]. Equating the expressions in equations 8 and 9 allows the numerical deduction of $\Delta\mu(v)$.

3. Diffusion coefficient calculations

The crux of this work is the refinement of PION's method for calculating the RF diffusion coefficient. PION has historically modelled this coefficient pitch angle averaged. To account for the pitch angle variation, we begin from Eq. 10, the pitch angle averaged form for D_{RF}:

$$D_{RF}(v) = \sum_N K \int_{-1}^{1} |E_+ J_{n-1}(k_\perp\rho) + E_- J_{n+1}(k_\perp\rho)|^2 d\mu \qquad (10)$$

Here K is a constant, and $\rho = \frac{v}{\omega_{ci}}\sqrt{1-\mu^2}$, the ion Larmor radius. Eq. 10 is given in this form in [6]. It has a longer history, being given in a more general context in [23].

We improve on Eq. 10 by applying the ansatz given in Eq. 7 to weight the diffusion operator average according to the distribution in μ, obtaining Eq. 11, the pitch angle resolved equation:

$$D_{RF}(v) = \sum_N K \int_{-1}^{1} \left|\frac{f(v,\mu)}{F(v)}(E_+ J_{n-1}(k_\perp\rho) + E_- J_{n+1}(k_\perp\rho))\right|^2 d\mu \qquad (11)$$

where the ratio of distribution functions is taken from the assumed angular distribution given in Eq. 7. The effect is to weight the contribution to the equation by particle density according to the pitch angle. The former version of the calculation, in making an average over the angle, takes the intermediate functional form Eq. 10, equivalent to Eq. 11 with $f(v,\mu) = F(v)$. Eqs. 10 and 11 indicate that D_{RF} is influenced by the Bessel functions that capture Finite Larmor Radius (FLR) effects, generating *v*-space structure including minima in $D_{RF}(v)$. To calculate the angle-resolved distribution function used in Eq. 11, PION first calculates the 1-D distribution function $F(v)$, and then converts this into a 2-D v-space distribution $f(v,\mu)$ using the Ansatz in Eq. 7.

In consequence of Eqs. 10 and 11, energy plots of D_{RF} bear a strong resemblance to Bessel functions, with a near-zero minimum. The location and depth of these minima are critical in determining the quasi-linear term of the Fokker-Planck equation, and hence the rate at which the tail of the distribution function f drops off with *v*. We see that the angular distribution presented here has implications for the location of this minimum: the treatment of the angle smears the Bessel function argument $k_\perp\rho$ across the range of values spanning from zero up to its value at $\mu = 0$. This alters both energy and RF diffusion coefficient minimum position values. Fig. 2 shows characteristic curve shapes, produced with typical experimental parameters. The constant form (Eq. 1), without angle treatment follows the form of its Bessel function inputs, with a series of zero minima, while the angle-averaged form (Eq. 10) has only weak minima, at somewhat increased energy values. Resolving the angle (Eq. 11) produces an intermediate case, due to the weighting in μ.

Fig. 3 compares the effect of averaging and resolving the pitch angle in this way for a pulse that will be considered in Sec. 4. We see in this example a decrease in the first non-zero energy location of a D_{RF} minimum, from 2.47 to 2.23 MeV, as well as a deeper minimum; the combination results in a markedly steeper tail to the distribution function, as we would expect.

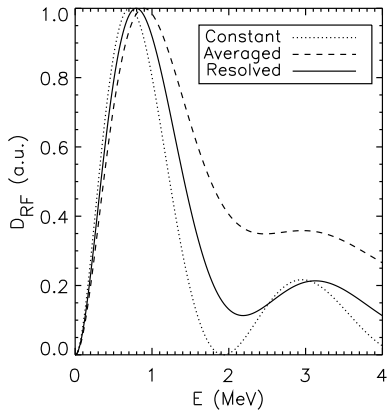

Figure 2: Typical variation of RF diffusion coefficient for the three formulations of the pitch angle. Parameters used: deuterium third harmonic, $k_\perp = 56.6\ m^{-1}$, $\frac{E_+}{E_-} = 0.43$, $\omega_c = 51.5\ MHz$.

Concluding this general analysis, we see several important variables between them determining the location of the diffusion coefficient first post-peak minimum. Both harmonic number and ion mass play key roles, as shown in Fig. 1 for the constant case, without angular dependence, the harmonic number in the orders of the Bessel functions, and the ion mass in the scaling of the energy axis. As the harmonic number increases, and as the ion mass decreases, the energy value of the first coefficient minimum reduces to experimentally

measurable values. Two more parameters play key roles in determining D_{RF}. The perpendicular wavenumber $k_\perp$ scales the arguments of the two Bessel functions, and the ratio of electric field polarisations E_+/E_- relatively weights the two Bessel functions against each other. The effects of these two parameters are important in general to this calculation, but not in specific to the scope of this study.

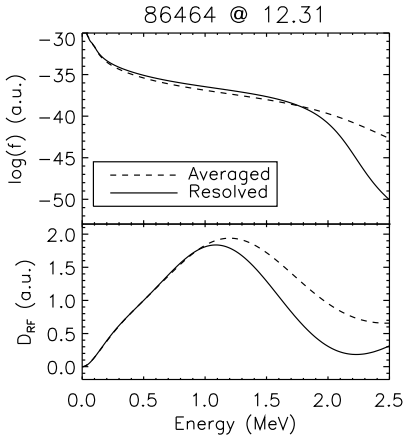

Figure 3: Variation of (above) distribution function f, and (below) RF diffusion coefficient for JET pulse 86464 at 12.31s

4. Comparison for specific experiments

4.1 Second harmonic heating of hydrogen

As illustrated in Fig. 1, to find differences in D_{RF} and hence distribution function tail it is of advantage to look beyond the common fundamental heating scheme. For hydrogen plasma, we see these differences in second harmonic heating schemes. In demonstration, we consider a JET pulse studied in [11], 58738, which utilised this heating scheme as part of an experimental campaign studying the interactions of FLR effects with the high energy distribution tail. The heating of this pulse is hydrogen minority in deuterium

We can compare PION's hydrogen distribution function with the output from the High Energy Neutral Particle Analyser (NPA) [34], output which was for these pulses presented in [11]. Modelling pitch angle dependence to compute D_{RF} gives the expected clear improvement in simulation-to-experimental matching of the distribution tail for this case, as shown in Fig. 4.

The implemented pitch angle resolution has no significant effect on the heated ion species power partition for this case. We see only a small change in power partition with the pitch angle resolution, a 2.0% increase, from 3.04 MW hydrogen absorption to 3.10 MW, with absorption by deuterium, the majority and next strongest absorbing species, lower by five orders of magnitude.

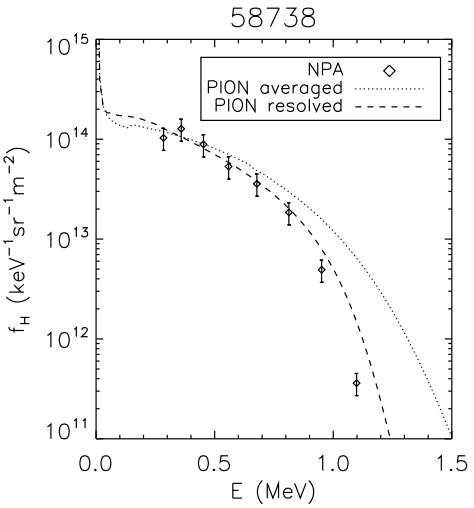

Figure 4: Hydrogen distribution functions f_H as given by PION without and with pitch angle resolution at t = 23 s and the same as deduced from High Energy NPA measurements [34] (integrated in time from t = 22.5 to 23.5 s) for JET discharge 58738 with second harmonic heating of hydrogen

4.2 Third harmonic heating of deuterium

For the case of third harmonic heating of deuterium, we re-examine JET pulses previously considered from a PION modelling perspective in [22, 32], 86459 and 86464. These pulses are from experiments dedicated to enhanced fusion production from deuterium-deuterium reactions [35]. Third harmonic heating of the deuterium population avoids both the heating of low energy particles found in fundamental heating and the interference of competing fundamental hydrogen heating found in second harmonic deuterium heating. This scheme was used to create a population of deuterium ions in the MeV energy range to match the peak of the D-D reaction cross-section. This method produces a high energy tail to the deuterium distribution, precisely the condition of interest to this work.

Fig. 5a shows the spatially averaged energy distribution function as given by PION using the pitch angle resolved ICRF diffusion coefficient calculation, comparing them with the experimental distribution functions for these discharges. The experimental distributions are those deduced from the 2.5 MeV TOFOR neutron spectrometer [36]. The TOFOR line of sight is vertical, and so it largely observes trapped populations, corresponding to μ values close to zero.

We observe a good agreement in Fig. 5a between the modelled and experimental distribution functions in the region of the high-energy tail. The corresponding ICRF diffusion coefficients are shown in Fig. 5b. We note the locations of the diffusion coefficient minima in the regions of the strong decays in the distribution functions, as expected. We note also that in Fig. 5a we can see that the agreement in the low energy

range, where pitch angle scattering becomes important, is less good. There are various candidate reasons for this, for example the low v pitch angle scattering resulting in $f(v,\mu)$ being more independent of μ at lower energy, departing from the assumption of Eq. 7. Other candidate reasons include simplifications used in the PION physical models and larger sensitivities in this energy range to uncertainties in the measured input data used in the modelling. The detailed investigation of these effects is beyond the scope of the present study, in which our focus is on the details of the high energy part of the distribution function. Nevertheless, we can see that PION is still able to also reproduce the measured trends in the low energy region; the PION distribution function for discharge 86459 always remains larger than that for discharge 86464, consistent with the measured trend.

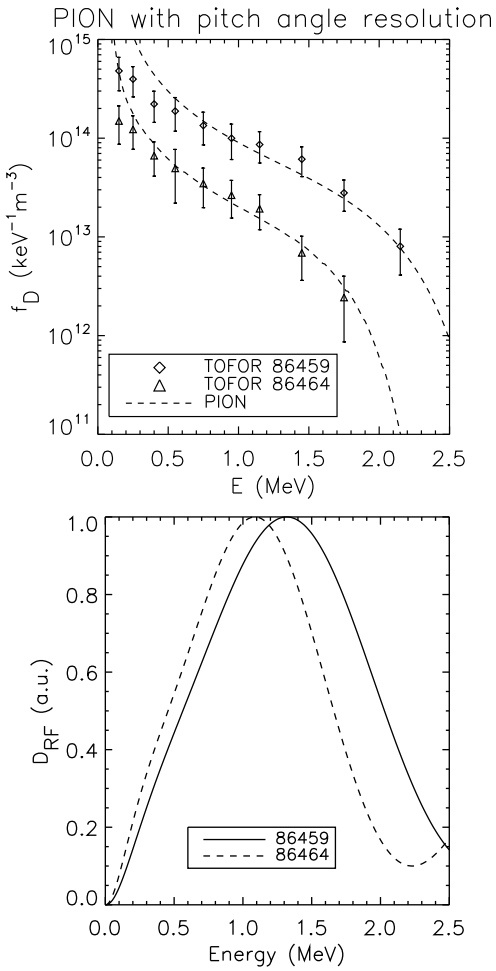

Figure 5: a) Deuterium distribution function f_D as given by PION at t = 12.3s and the same as deduced from the TOFOR [36] measurements (diamonds and triangles; integrated in time from t = 11.5 to 12.5 s) for JET discharges 86459 and 86464 at 12.31s with third harmonic heating of deuterium and angular resolution of the RF diffusion coefficient; b) RF diffusion coefficients for these two cases.

The third harmonic deuterium heated pulses show a significant change in ion power absorption. The third harmonic deuterium scheme avoids overlap with hydrogen harmonics, and so there is no transfer of power between species. Rather, we see modelled enhancement to the deuterium heating, as shown in Table 1. In the PION modelling of these pulses, we have included a parasitic damping effect as used in earlier modelling of the same discharges [32], where an assumed percentage of wave energy is damped at the plasma edge by other species. This technique is used because it has previously been demonstrated necessary for accurate PION power partition results for these third harmonic deuterium heating cases [37]. The changes in Deuterium absorbed power shown in Table 1 result from power previously parasitically absorbed now being absorbed by Deuterium.

86459	*Power to D (MW)*
Pitch angle averaged	*1.41*
Pitch angle resolved	*1.77*

86464	*Power to D (MW)*
Pitch angle averaged	*1.35*
Pitch angle resolved	*2.05*

Table 1: Power absorbed by deuterium as given by PION for (above) 86459 and (below) 86464

5. Conclusions

A refinement to the modelling of the RF diffusion operator in the PION code has been implemented and its results compared for JET cases where the changes were expected to be of significance. This refinement consists of including a physics-based Ansatz for the fast ion distribution function dependence on pitch angle, instead of an averaging process assuming this is uniform. We have observed improved agreement between the modelled distribution function and measurements in the high energy tail in hydrogen and deuterium plasmas with higher harmonic heating schemes. We have also observed changes to the power absorption as a result of this modification.

While offering improved analysis of existing pulses in the JET data library, this refinement also has relevance to analyses on future devices. For example, among the current ITER scenarios, there are three that utilise second harmonic hydrogen heating, labelled T.a, T.b, and T.c; these are the so-called "third-field" cases, labelled "T" because B_0 is one third of the full available ITER B_0. These have been analysed with

PION in [21], in which parameters are given that are sufficient for the calculation of generic diffusion coefficient energy profiles for these scenarios, as in Fig. 2.

On producing these profiles in pitch angle resolved form, we see that cases T.b and T.c both exhibit diffusion coefficient minima in the low MeV range, as shown in Fig. 6. We also see in comparing the pitch angle averaged and resolved versions of D_{RF} that the minimum is much less present in the averaged version, especially for T.b. This is precisely the behaviour that makes the angular dependence as documented in this paper important in calculating the distribution tail. This modelling refinement will be important for these scenarios, and the planned gamma-ray diagnostics for ITER [38, 39] will provide experimental data to verify against.

The precise effect on global quantities is hard to predict in general terms, given the non-linear nature of ICRF physics. Power partitioning between the plasma ion species is a complex phenomenon, with multiple possible absorptions – in addition to the specific species absorption targeted in a given pulse, other species may also see significant resonances. There may be parasitic resonances, as included in this modelling for 86459 and 86464. There will also be direct electron absorption. For the three JET discharges described in this paper, we observed variable increases in the power absorbed by the resonant ion species, covering the range 2-51%. It is to be expected that the impacts of including these effects will be similar on ITER.

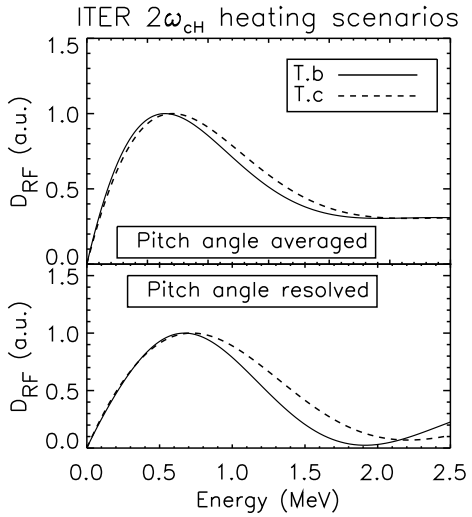

Figure 6: RF diffusion coefficients for selected ITER scenarios calculated with (above) pitch angle averaged and (below) pitch angle resolved

Acknowledgements

The CCFE part of this work has been carried out within the framework of the EUROfusion Consortium and has received funding from the Euratom research and training programme 2014-2018 and 2019-2020 under grant agreement No 633053. The views and opinions expressed herein do not necessarily reflect those of the European Commission.

The BSC part of this project is co-financed by the European Union Regional Development Fund within the framework of the ERDF Operational Program of Catalonia 2014-2020 with a grant of 50% of total cost eligible.

The authors are grateful to Paula Siren and Jacob Eriksson for assistance with experimental data, to Lars-Göran Eriksson for discussions on the implementation of the new features, and to Colin Roach and Michael Fitzgerald for valuable comments on the manuscript.

References

[1] J. Ongena et al. 2017 *Plasma Phys. Control. Fusion* **59** 054002
[2] J. R. Wilson and P. T. Bonoli 2015 *Phys. Plasmas* **22** 021801
[3] J.-M. Noterdaeme 2020 *AIP Conference Proceedings* **2254**, 020001
[4] L.-G. Eriksson and T. Hellsten 1995 *Physica Scripta* **52**, 70-79
[5] L.-G. Eriksson, T. Hellsten and U. Willén, 1993 *Nucl. Fusion* **33** 1037.
[6] M. J. Mantsinen, 1999 *Development and Experimental Evaluation of Theoretical Models for Ion Cyclotron Resonance Frequency Heating of Tokamak Plasmas* Helsinki University of Technology, ISBN 951-22-4460-8
[7] D.F.H. Start et al. 1998 *Phys. Rev. Lett.* **80** 4681
[8] D.F.H. Start et al. 1999 *Nucl. Fusion* **39** 321
[9] J. Garcia et al. 2017 *Plasma Phys. Control. Fusion* **59** 014023
[10] M.J. Mantsinen et al. 2002 *Phys. Rev. Lett.* **88:10** 105002
[11] A. Salmi et al. 2006 *Plasma Phys. Control. Fusion* **48** 717
[12] M.J. Mantsinen et al. 2001 *Nucl. Fusion* **41(12)** 1815
[13] D. Gallart et al. 2018 *Nucl. Fusion* **58** 106037
[14] M.J. Mantsinen et al. 2015 *AIP Conference Proceedings* **1689** 030005
[15] M.J. Mantsinen et al. 2016 *43rd EPS Conference on Plasma Physics* **40A** 030005
[16] M. García-Muñoz et al. *Phys. Rev. Lett.* **100(5)** 055005
[17] S.E. Sharapov et al. 2017 *Plasma Phys. and Control. Fusion* **60(1)** 014026
[18] M. J. Mantsinen et al. 2002 *Physics of Plasmas* **9** 1318
[19] L.-G. Eriksson et al. 2017 *Physics of Plasmas* **24** 022122
[20] A. Becoulet et al. 2000 *J. Plasma Fusion Res.* **3** 51–57
[21] I.L. Arbina et al. 2019 *Proc. 46th EPS Conf. Plasma Physics* **P4** 1079
[22] M. Schneider et al. 2016 *Nucl. Fusion* **56** 112022
[23] C.F. Kennel and F. Engelmann 1966 *Phys. Fluids* **9** 2377 40
[24] L.-G. Eriksson et al. 1994 *Phys. Plasmas* **1** 308
[25] X. Llobet et al. 1988 *Theory of Fusion Plasmas (Proceedings of the Joint Varenna-Lausanne International Workshop, Chexbres)* Editrice Compositori, Bologna 663
[26] L. Villard et al. 1996 *Computer Physics Reports* **4** 95
[27] K.G. Budden 1961 *Radio Waves in the Ionosphere*. CUP, Cambridge, 1961, ISBN 0-521-25461-2
[28] L.-G. Eriksson et al. 1999 *Phys. Rev. Lett.* **81(6)** 1231
[29] T. H. Stix 1972 *Plasma Physics* **14** 367
[30] D. Anderson et al. 1987 *Nucl.. Fusion* **27** 911

[31] T. H. Stix 1992 *Waves in Plasmas* American Institute of Physics, ISBN 978-0-88318-859-0
[32] M. J. Mantsinen et al. 2015 *IAEA Technical Meeting n Energetic Particles (Vienna)* http://www-naweb.iaea.org/napc/physics/meetings/TM49508/website/Papers/Mantsinen%20M.pdf
[33] D. Anderson et al. 1987 *Plasma Phys. Control. Fusion* **29** 891
[34] A.A. Korotkov et al. 1997 *Nucl. Fusion* **37** 35
[35] S. E. Sharapov et al. 2016 *Nucl. Fusion* **56** 112021
[36] M. Gatu Johnson et al. 2008 *Nucl. Instrum. Methods A* **591** 417
[37] L.-G. Eriksson et al. 1998 *Nucl. Fusion* **38** 265
[38] V.G. Kiptily et al. 2006 *Plasma Phys. Control. Fusion* **48** R59
[39] I.N. Chugunov et al. 2011 *Nucl. Fusion* **51** 083010